ADVANCED MATERIALS
www.advmat.de

Check for updates

Gigantic Current Control of Coercive Field and Magnetic Memory Based on Nanometer-Thin Ferromagnetic van der Waals Fe_3GeTe_2

Kaixuan Zhang, Seungyun Han, Youjin Lee, Matthew J. Coak, Junghyun Kim, Inho Hwang, Suhan Son, Jeacheol Shin, Mijin Lim, Daegeun Jo, Kyoo Kim, Dohun Kim, Hyun-Woo Lee,* and Je-Geun Park**

Controlling magnetic states by a small current is essential for the next-generation of energy-efficient spintronic devices. However, it invariably requires considerable energy to change a magnetic ground state of intrinsically quantum nature governed by fundamental Hamiltonian, once stabilized below a phase-transition temperature. Here, it is reported that, surprisingly, an in-plane current can tune the magnetic state of the nanometer-thin van der Waals ferromagnet Fe_3GeTe_2 from a hard magnetic state to a soft magnetic state. It is a direct demonstration of the current-induced substantial reduction of the coercive field. This surprising finding is possible because the in-plane current produces a highly unusual type of gigantic spin–orbit torque for Fe_3GeTe_2. In addition, a working model of a new nonvolatile magnetic memory based on the principle of the discovery in Fe_3GeTe_2, controlled by a tiny current, is further demonstrated. The findings open up a new window of exciting opportunities for magnetic van der Waals materials with potentially huge impact on the future development of spintronic and magnetic memory.

Dr. K. Zhang, Y. Lee, Dr. M. J. Coak, J. Kim, I. Hwang, S. Son, Prof. J.-G. Park
Center for Correlated Electron Systems
Institute for Basic Science
Seoul 08826, South Korea
E-mail: kxzhang@snu.ac.kr; jgpark10@snu.ac.kr

Dr. K. Zhang, Y. Lee, Dr. M. J. Coak, J. Kim, I. Hwang, S. Son, J. Shin, Prof. D. Kim, Prof. J.-G. Park
Department of Physics and Astronomy
and Institute of Applied Physics
Seoul National University
Seoul 08826, South Korea

Dr. K. Zhang, Y. Lee, J. Kim, I. Hwang, S. Son, Prof. J.-G. Park
Center for Quantum Materials
Seoul National University
Seoul 08826, South Korea

S. Han, M. Lim, D. Jo, Prof. H.-W. Lee
Department of Physics
Pohang University of Science and Technology
Pohang 37673, South Korea
E-mail: hwl@postech.ac.kr

Dr. K. Kim
Korea Atomic Energy Research Institute
111 Daedeok-daero, Daejeon 34057, South Korea

Prof. H.-W. Lee
Asia Pacific Center for Theoretical Physics
77 Cheongam-ro, Nam-gu, Pohang 3773, South Korea

The ORCID identification number(s) for the author(s) of this article can be found under https://doi.org/10.1002/adma.202004110.

DOI: 10.1002/adma.202004110

The last few years have witnessed that the new arrival of 2D magnetic van der Waals (vdW) materials have attracted colossal attention worldwide.[1–6] When combined with a wide variety of other 2D nonmagnetic vdW materials,[7] these magnetic vdW materials can open up a new horizon of novel nanoelectronic devices[8–11] that consist entirely of 2D materials. Among all the magnetic vdW materials, Fe_3GeTe_2 (FGT) received special attention because it is the only topological ferromagnetic vdW metal.[12] The nanoscale FGT is a metallic hard ferromagnet with a large coercivity of approximately several kOe.[13] It exhibits a significant anomalous Hall effect (AHE),[12,14] allowing easy probing of its magnetic configurations via electrical transport measurements. Besides, exciting new behavior was also found in the FGT-based heterostructure, such as the unconventional 3-state magnetoresistance.[15]

Electrical modulation of the magnetic anisotropy or coercivity is critical to realizing energy-efficient spintronic devices such as memory. For information storage, the magnetic anisotropy should be high enough to minimize the information loss by fluctuations. In contrast, the magnetic anisotropy should be small for information writing with low energy consumption, which is desirable for any energy-efficient device. These self-contradicting conditions require that the anisotropy should be able to be lowered only on demand (current applied for writing), and otherwise kept high enough to ensure the stability of the information stored (no current for storage). Here we provide the first experimental demonstration for such on-demand modulation of the coercivity and a working model of a magnetic memory in nm-thin FGT.

In this experiment, we discover that the coercive field H_c of FGT can be reduced by ≈50% (≈100%) by applying a tiny in-plane electric field of ≈0.1 mV nm^{-1} (≈0.3 mV nm^{-1}), respectively. In comparison, all the previous attempts used an out-of-plane electric field (often in the range of 0.1 V nm^{-1}), several orders of magnitude larger than ours, to induce a much smaller degree of modulation (e.g., <5% for FePt and FePd[16]): for example, semiconducting vdW magnets[17–20] and metallic magnetic thin films.[16,21] The coercivity modulation by an in-plane field has a drawback of energy dissipation. Nevertheless, our

 © 2020 Wiley-VCH GmbH

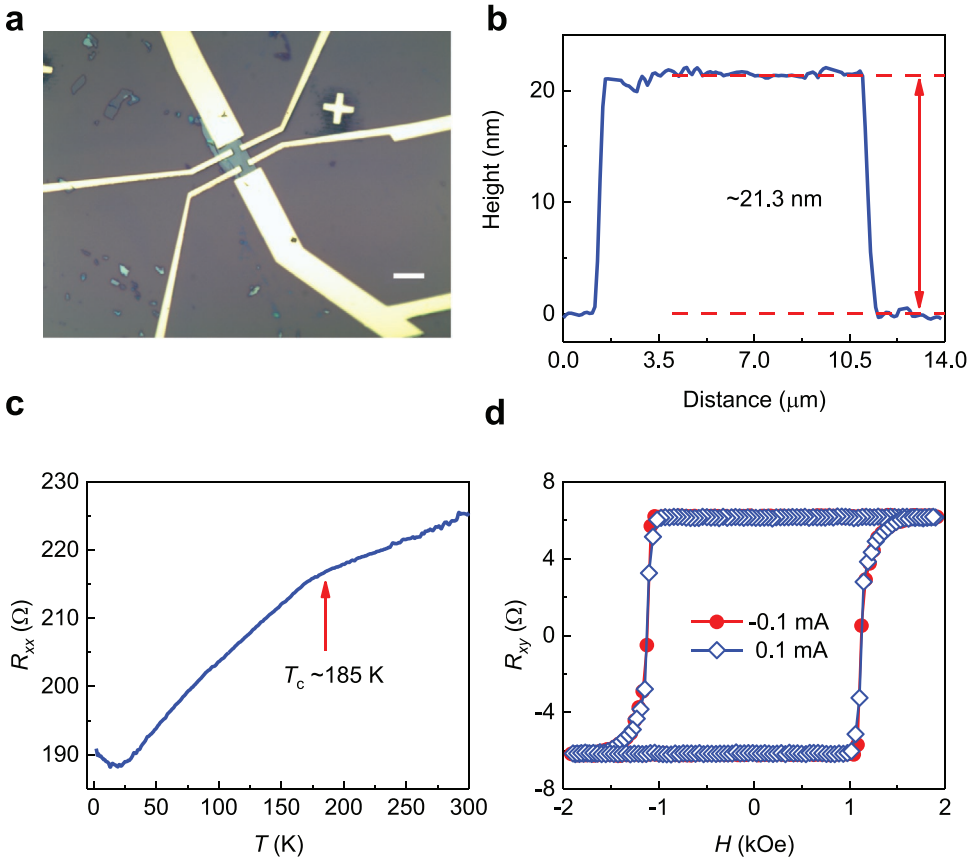

Figure 1. Sample preparation and transport measurements. a) Optical image of a typical FGT nanoflake sample (sample S1) with a Hall-bar geometry electrode. The white scale bar represents 10 μm. b) The thickness of sample S1 is 21.3 nm, as measured by AFM. c) Longitudinal resistance R_{xx} as a function of temperature T with current $I = 0.05$ mA. The red arrow indicates the magnetic transition due to spin-flip scattering, from which $T_c \approx 185$ K is determined. d) Hall resistance R_{xy} as a function of magnetic field H at 2 K with $I = +0.1$ mA and -0.1 mA.

result of the monotonic modulation of the coercivity provides a promising alternative for electrical modulation. It requires neither a complicated ionic-liquid gating[14] nor a very high gating voltage[17–21] (generally >30 V). Moreover, while the out-of-plane field case depends on a field-induced change of carrier density[16–20] or orbital occupation,[21] we find that the electrical modulation of H_c observed in FGT is strongly influenced by the spin–orbit torque (SOT)[22–24] induced by an in-plane electric current. The SOT is a current-generated torque acting on a magnetic order and usually generated by an in-plane current flowing in heavy metal (such as Pt and Ta) in contact with magnets.[22,25,26] In FGT, on the other hand, an in-plane current in FGT itself generates the SOT[27] owing to the particular geometrical structure of FGT. We estimate that the effective magnetic field due to the SOT is on the order of 50 Oe for a small current density of 1 mA μm^{-2}, which is about two orders of magnitude larger than that produced by heavy metals like Pt and Ta.[28] We further reveal that the large SOT is due to the large Berry curvature in the topological ferromagnetic metal FGT. Based on these observations, a prototypical nonvolatile magnetic memory of high energy-efficiency is further demonstrated in this work.

FGT single crystals were grown by the chemical vapor transport method and adopted for the device fabrication (see the Experimental section). Our bulk FGTs are hole-doped Fe_xGeTe_2 with x varying from 2.77 to 2.89 according to the energy-dispersive X-ray spectroscopy (EDS) measurements. We made several FGT devices with different thicknesses (samples S1, S2, S3, S4, S5, and S6 with a thickness of 21.3, 16.7, 6, 42, 17.5, and 15 nm, respectively). **Figure 1**a shows a typical FGT device (sample S1) with electrodes of a Hall bar geometry. The thickness is measured to be 21.3 nm by the atomic force microscopy (AFM) in Figure 1b. Figure 1c displays the longitudinal resistance (R_{xx}) of FGT as a function of temperature T. The R_{xx}–T curve exhibits the spin-flip scattering-induced magnetic transition with $T_c \approx 185$ K and the Kondo-like minimum at ≈20 K, both of which are the typical features of FGT.[13] Figure 1d depicts the transverse Hall resistance (R_{xy}) of FGT as a function of an out-of-plane magnetic field (H). The almost rectangle-shaped sharp hysteresis loop in the R_{xy}–H curve confirms that FGT is indeed a hard magnet: the dominant contribution to R_{xy} comes from the AHE[12,14] while the ordinary Hall effect is negligible. The H_c of all our FGT nanoflakes varies from 1 to 2.2 kOe, which is indicative of hole-doped Fe_xGeTe_2 with $2.7 < x < 3$ according to previous investigations,[13,29] and thus consistent with the EDS results.

Interestingly, H_c of the hysteresis loop gets significantly reduced as an in-plane current I applied to FGT increases from 0.05 to 1.5 mA (**Figure 2**a). On the other hand, the remnant Hall resistance R_{xy}^r remains almost unchanged with I, implying that the saturation magnetization of FGT is not much affected by I. Thus, I reduces H_c without disrupting the

© 2020 Wiley-VCH GmbH

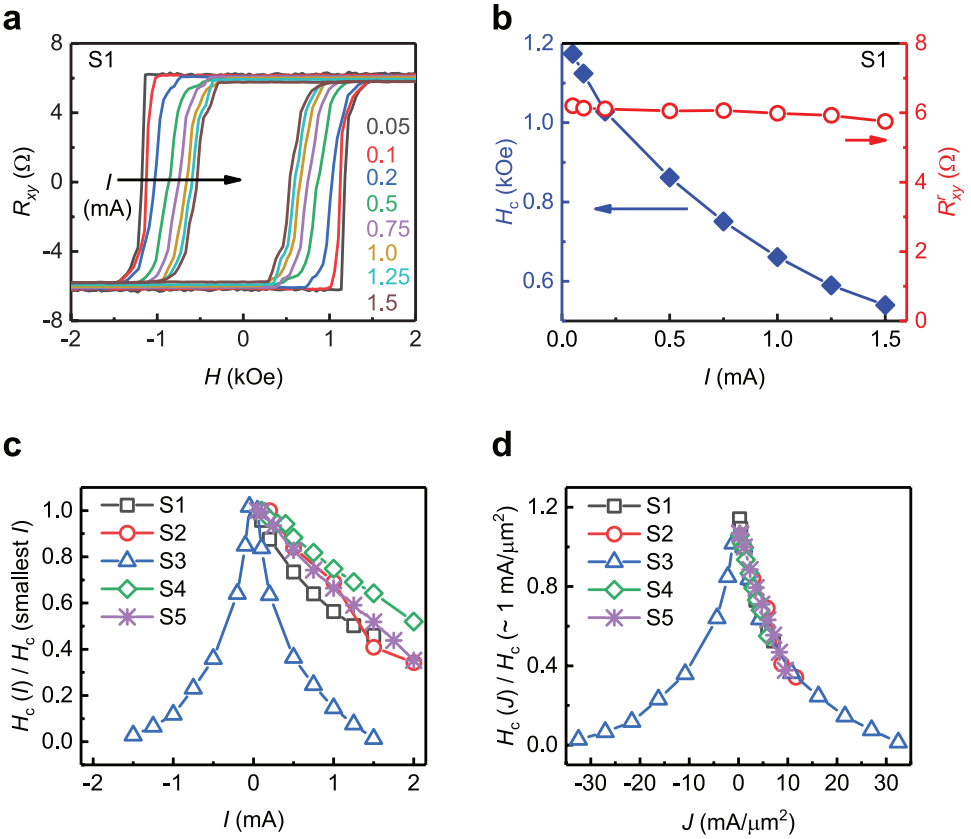

Figure 2. Current-dependent magnetism. a) R_{xy}–H curves of sample S1 at 2 K with applied current I varying from 0.05 to 1.5 mA. b) Extracted coercive field H_c and remnant Hall resistance R_{xy}^r of sample S1 as a function of applied current I at 2 K. c) $H_c(I)/H_c$ (smallest I) as a function of applied current I for sample S1 (21.3 nm; black squares), S2 (16.7 nm; red circles), S3 (6 nm; blue triangles), S4 (42 nm; green diamonds), and S5 (17.5 nm; purple stars) at 2 K. d) $H_c(J)/H_c(\approx 1\ \text{mA}\ \mu\text{m}^{-2})$ as a function of current density J for sample S1, S2, S3, S4, and S5 at 2 K.

ferromagnetic ordering of FGT, which is ideal for spintronic device applications. H_c and $R_{xy}{}^r$ of the sample S1 are shown in Figure 2b as a function of I. Note that the current of 1.5 mA reduces H_c by more than 50% (cf. <5% for FePt and FePd[16]). We also measured several other samples (samples S2, S3, S4, and S5) with a similar reduction of H_c by I (Figure S1 for sample S2, Figures S2 and S3 for sample S3, Figure S4 for sample S4, and Figure S5 for sample S5, Supporting Information). The current dependence of H_c for all the samples is summarized in Figure 2c. Figure 2d displays the normalized H_c as a function of current density J, where H_c is normalized by its value at small J (≈1 mA μm^{-2}). As can be seen, the current reduces H_c by ≈50% for ≈7 mA μm^{-2} (corresponding to ≈0.07 mV nm^{-1}) and ≈100% for ≈30 mA μm^{-2} (corresponding to ≈0.3 mV nm^{-1}).

The H_c reduction by the current can arise partly by the Joule heating since H_c gets reduced at higher temperatures. We adopt three different methods to quantify the Joule heating contribution to the H_c reduction. After comprehensive and systematic studies as summarized in the Supporting Information, we conclude that the Joule heating is responsible only for 30% (thickest sample S4) to 60% (thinnest sample S3) of the total H_c reduction at $J \approx 10$ mA μm^{-2}. It implies that roughly half of the reduction experimentally observed is due to a non-Joule-heating effect of nontrivial origin.

We would now like to examine how the non-Joule-heating effect can arise from the SOT. We demonstrate below the effective field due to the SOT in FGT is about two orders of magnitude larger than those values reported before for heavy metals such as Pt.[28] An in-plane current density $J = (J_x, J_y, 0)$ generates the SOT $T_{SOT} = -|\gamma| M \times H_{SOT}$ acting on the magnetization $M = (M_x, M_y, M_z)$, where $|\gamma|$ is the gyromagnetic ratio. The symmetries of a given system constrain the structure of the effective field H_{SOT} in T_{SOT}. **Figure 3**a shows the crystal structure of a monolayer Fe_3GeTe_2 with the distinct three symmetries: the three-fold rotation symmetry around the c-axis (z-axis), the mirror reflection symmetry with respect to the a-axis (y-axis), and the mirror reflection symmetry with respect to the c-axis. Under this set of symmetries, the general form of H_{SOT} can be expressed as;[27]

$$H_{SOT} = \Gamma_0 \left[\left(m_x J_x - m_y J_y \right) \hat{\mathbf{x}} - \left(m_y J_x + m_x J_y \right) \hat{\mathbf{y}} \right] \tag{1}$$

where $m = (m_x, m_y, m_z) = \text{M}/|\text{M}|$ and Γ_0 is a coefficient that parametrizes a magnetoelectric coupling strength. Unlike H_{SOT} in other systems, the effective field H_{SOT} of FGT is conservative[27] and can be obtained from an effective free energy density f_{SOT} by $H_{SOT} = -\partial f_{SOT}/\partial M$ with

$$f_{SOT} = M_s \Gamma_0 \left[J_y m_x m_y - \frac{1}{2} J_x \left(m_x^2 - m_y^2 \right) \right] \tag{2}$$

© 2020 Wiley-VCH GmbH

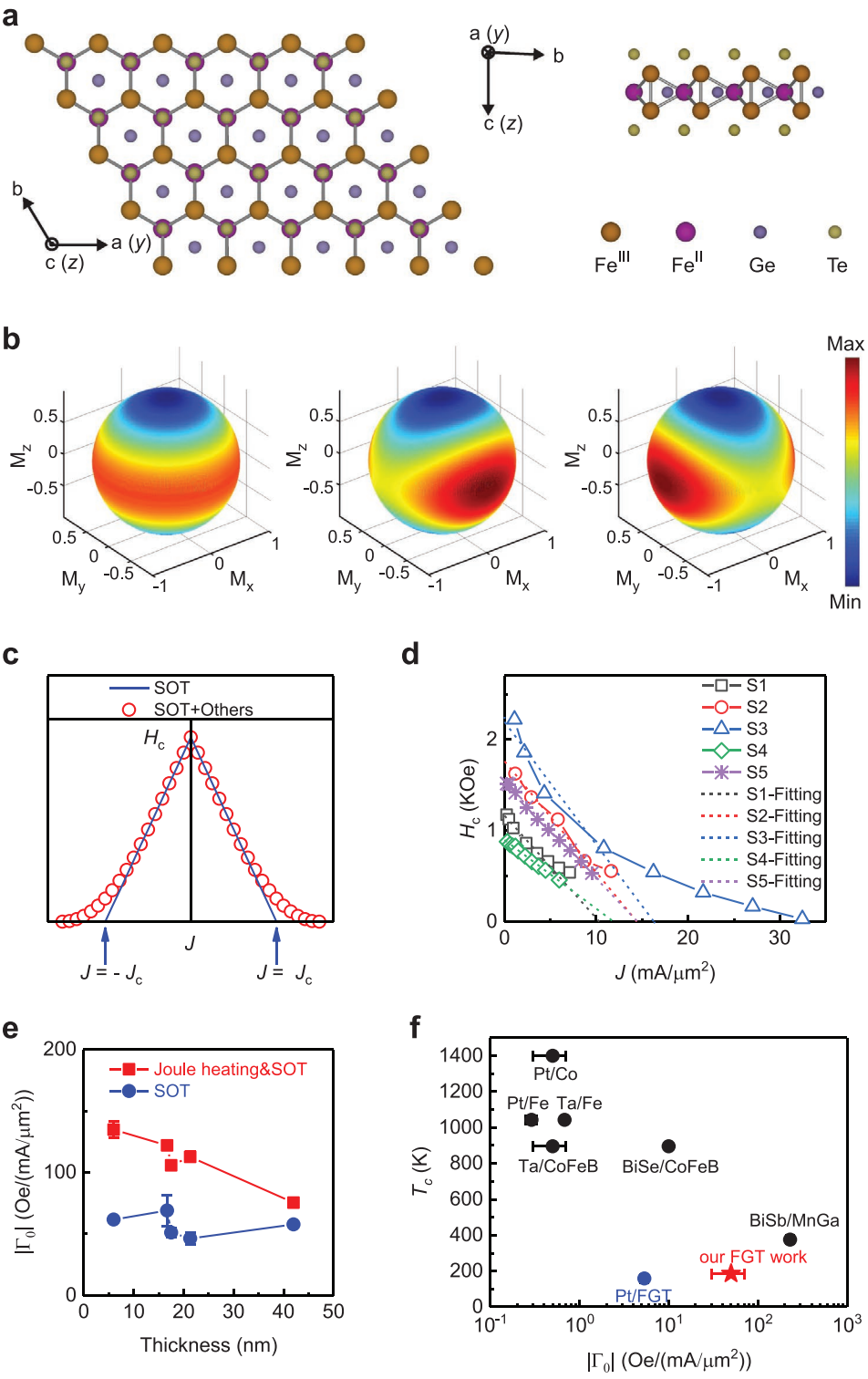

Figure 3. Analysis based on the spin–orbit torque of FGT. a) The crystal structure of a monolayer Fe_3GeTe_2. Left: View along the *c* axis; right: view along the *a*-axis. Fe^{III} and Fe^{II} denote the two inequivalent Fe sites with oxidation number +3 and +2, respectively. b) Free energy profiles for $J = 0$ (left), J type $= J > 0$ (middle), and $J < 0$ (right). c) Theoretical curves for the coercivity H_c as a function of the current density J. The solid blue lines indicate the results due to the SOT. In contrast, the open red circles indicate the results due to both SOT and other mechanisms, e.g., magnetic dipolar interaction between neighboring domains. d) Experimental H_c–J curves at 2 K for sample S1 (black squares), S2 (red circles), S3 (blue triangles), S4 (green diamonds), and S5 (purple stars). The dashed lines denote the corresponding linear fitting lines within a relatively small J range. e) Estimated $|\Gamma_0|$ for the SOT contribution alone (blue circles) and the combined case of both Joule-heating-effect and SOT contribution (red squares) as a function of the sample thickness. f) The values of $|\Gamma_0|$ and T_c from our FGT samples and various composite SOT systems.[25,28,35,41]

© 2020 Wiley-VCH GmbH

It implies that the SOT effect in FGT amounts to the magnetic anisotropy change, whereas such an interpretation is not possible for the damping-like SOT in other systems. This structure of f_{SOT} derived for a monolayer FGT is also applicable to each layer of a multilayer FGT like our samples since each layer satisfies the symmetries, and the interlayer coupling is weak in the vdW FGT[30,31] (see more details in the Note S3, Supporting Information). Together with the inherent free energy density $f_0 = -(1/2)K_z M_z^2 / M_s$ that describes the Ising-type perpendicular magnetic anisotropy of FGT, one obtains the effective free energy density $f_{eff} = f_0 + f_{SOT}$ in the presence of current as follows:

$$f_{\text{eff}} = -\frac{M_s}{2}\left[K_z \cos^2\theta + \Gamma_0 J \sin^2\theta \cos\left(2\phi + \phi_J\right)\right] \tag{3}$$

where the angles θ and ϕ specify the directions of the unit vector $m = (\sin\theta\cos\phi, \sin\theta\sin\phi, \cos\theta)$, and $J = J(\cos\phi_J, \sin\phi_J, 0)$.

We now demonstrate how J can effectively reduce the barrier height between the local minima of the free energy. Figure 3b shows our theoretical calculations for the effective free energy density f_{eff} profile when the current is applied along the armchair direction ($\phi_J = 0$). For $J = 0$, f_{eff} has a minimum value of $-M_s K_z/2$ at $m = \pm\hat{\mathbf{z}}$ and a maximum value of 0 when m lies in the xy plane (left panel). Thus to switch the magnetization from $m = -\hat{\mathbf{z}}$ to $m = +\hat{\mathbf{z}}$, one should overcome the free energy barrier of $M_s K_z/2$. Then the f_{eff} profile for $\Gamma_0 J > 0$ (middle panel) shows that interestingly the free energy barrier along $m = \pm\hat{\mathbf{x}}$ is decreased. Although the barrier is increased along $m = \pm\hat{\mathbf{y}}$, this increase is irrelevant since a magnetic switching occurs through a path that minimizes the energy barrier, which in this case is $m = -\hat{\mathbf{z}} \rightarrow \pm\hat{\mathbf{x}} \rightarrow +\hat{\mathbf{z}}$. Likewise, the f_{eff} profile for $\Gamma_0 J < 0$ (right panel) exhibits that the free energy barrier is lowered along $m = \pm\hat{\mathbf{y}}$, resulting in the switching along the path $m = -\hat{\mathbf{z}} \rightarrow \pm\hat{\mathbf{y}} \rightarrow +\hat{\mathbf{z}}$. A simple analysis shows that J modifies the free energy barrier from $M_s K_z/2$ to $M_s K_z/2 - M_s|\Gamma_0 J|/2$ (see the Experimental Section). The free energy barrier can be lowered further by H and vanishes when $H = K_z - |\Gamma_0 J|$. Thus H_c is given by $K_z - |\Gamma_0 J|$ for a single domain case. This analysis shows that H and $|\Gamma_0 J|$ play similar roles in the energy barrier. In an actual switching process, however, the switching can be more complicated due to the magnetic domains[32] in FGT, and the free energy barrier for $H = J = 0$ becomes smaller[33,34] than K_z. Although it is difficult to have an analytic evaluation of the free energy barrier, we can approximate it by the experimentally measured $H_c(J = 0)$ since H competes with the free energy barrier and makes the switching when $H = H_c(J = 0)$.[35] Considering that H and $|\Gamma_0 J|$ play similar roles for the energy barrier, $H_c(J)$ can be approximated by $H_c(J) = H_c(0) - |\Gamma_0 J|$ and we then obtain the theoretical prediction $H_c(0) - H_c(J) = \Delta H_c(J) = |\Gamma_0 J|$ (solid blue line in Figure 3c), which was also adopted in the previous studies.[35]

The predicted linear dependence on $|J|$ is roughly in agreement with the linear-in-J behavior of $\Delta H_c(J)$ (Figure 3d) in the relatively small J regime. By fitting the experimental result with the above formula, one obtains the first estimation of the spin–orbit field $|H_{SOT}| \sim |\Gamma_0 J|$, ranging from 75 to 135 Oe for $J = 1$ mA μm^{-2} (Figure 3e). It is an overestimation, however, since the H_c reduction is also partly due to the Joule heating. After carefully excluding the Joule-heating contribution, we obtain the refined and more realistic estimate of the non-Joule-heating contribution $|H_{SOT}| \sim |\Gamma_0 J|$, which is 50 ± 15 Oe for $J = 1$ mA μm^{-2} for all the samples (Figure 3e). Please note that this effective field strength (per J) is two orders of magnitude larger than that produced by heavy metals such as Pt and Ta,[28] and comparable only to that produced by the topological insulator BiSb[35] (Figure 3f). We also estimate $|H_{SOT}|$ independently by measuring the anisotropic magnetoresistance (AMR) as a function of an in-plane magnetic field direction. Since SOT makes the effective free energy dependent on the azimuthal angle of the magnetization (Figure 3b), the AMR can deviate from its conventional angular dependence. This predicted deviation is observed in our experiments, and by fitting the difference, one obtains $|\Gamma_0 J| \approx 119$ Oe for $J = 1$ mA μm^{-2} (Note S2, Supporting Information). To get further confidence in our analysis, we performed the first-principles calculation to evaluate the Berry curvature contribution to H_{SOT} (Note S3, Supporting Information) and obtain $|\Gamma_0 J| \approx 30$ Oe at $J = 1$ mA μm^{-2} for hole-doped Fe_xGeTe_2 with $2.7 < x < 3$. From these three independent analyses that produce similar estimations of Γ_0, we conclude that the non-Joule-heating-effect contribution to the current-induced H_c reduction arises from the SOT. It was reported[12] that FGT is a topological nodal-line semimetal with the topological band structure enhancing the Berry curvature contribution to the anomalous Hall effect. The considerable H_{SOT} value estimated from our analysis can share a similar origin. By the further comprehensive theoretical calculations and then careful comparison with the experimental results, we concluded that most of our observed SOT effects ought to be intrinsic (see more discussions in Note S3, Supporting Information). It is not easy to explicitly evaluate whether there is some remaining extrinsic disorder contribution[36] at present, which might be clarified in further study.

A recent experiment[25] on the FGT/Pt bilayer system measured the SOT magnitude of the bilayer. The result is one order larger than that produced by the conventional heavy metal Pt and one order smaller than the SOT in our present work (Figure 3f). We suspect that for the bilayer, both Pt and FGT may affect the measured SOT magnitude. Considering the current shunt in Pt, the intermediate SOT magnitude of FGT/Pt system between that produced by Pt and that produced by FGT provides a shred of consistent evidence for such conjecture.

When J becomes larger and closer to J_c ($\equiv H_c(0)/|\Gamma_0|$), i.e., the effective energy becomes small, multi-domain structure effect also gets severe during the magnetization switching. In such a situation, the hysteresis loop may be no longer as sharp as the case with a small current, consistent with the experimental results (Figure 2a and Figure S3, Supporting Information). In systems with the perpendicular magnetic anisotropy, magnetic dipolar interaction between neighboring domains can effectively reduce the magnetic field acting on the system, thereby enhancing H_c for bigger current. The red circles in Figure 3c depict the enhanced H_c, which is similar to the experimental result (Figure 3d).

Note that for conventional ferromagnetic materials like FGT, the magnetic anisotropy decreases as temperature increases, and thus the coercivity generally reduces upon increasing temperature.[13] Joule heating can enhance the temperature of the device and, therefore, can correspondingly reduce the

© 2020 Wiley-VCH GmbH

coercivity without requiring spin–orbit torques. However, the Joule heating effect frequently exists in many SOT systems[25] associated with large current. It is not suitable for device performance considering the stability of working temperature and the device aging problem, etc., although it can reduce the coercivity. Therefore, it is always valuable and desirable to find some new systems like FGT with large spin–orbit torques. On the other hand, for better practical application, we need to decrease or control the Joule heating effect of the device in the future.

Next, we demonstrate a new type of magnetic memory based on our observation of the giant current-controlled coercivity reduction in nanometer-thin vdW FGT. **Figure 4**a shows the schematic of the magnetic memory device, where the information can be easily written by writing the current I_{write} and read through R_{xy}. For instance, when the device is initially in the "0" state, we can alter it to the "1" state through the writing path I: we first turn on a small H in the order of 100 Oe (e.g., 850 Oe) then apply a I_{write} (Figure 4b). Since H_c is significantly reduced by I_{write}, the magnetization of the FGT device can be switched by current from "0" to "1" states above certain critical current.

Figure 4c shows the measured Hall voltage (V_{xy}) as a function of I_{write} (0 → 2→ −2 → 2 mA) under various H from −0.5 to 0.5 T. From these $V_{xy}(H)$ − I_{write} curves, we define $R_{xy}(H)$ − R_{xy}(−0.5 T) as ($V_{xy}(H)$ − V_{xy}(−0.5 T))/I_{write}, and the converted results are shown in Figure 4d. It is clear that initially, the FGT device is robustly in the "0" state ("$-M_s$" state) regardless of current sweep under −0.5, and 0 T; then under 0.085 T, when I_{write} increases from 0 to 2 mA, the magnetization gradually increases to "$+M_s$" (indicated by the blue arrow), i.e., to the "1" state. It is noteworthy that after reaching the "1" state, the magnetization is well maintained while sweeping the current. It proves that such magnetic information transition from "0" to "1" states through I_{write} is robust and nonvolatile.

Although still prototypical, we can emphasize several significant merits of the FGT-based device. First and foremost, it is a first working memory device entirely based on the vdW topological ferromagnetic metal (FGT) with the unusual type of gigantic SOT. Second, thanks to the matured technique for 2D materials, FGT-based devices can, in principle, be fabricated without undesired defects, including many grain boundaries and point defects, which are easily introduced during the growth and annealing processes for the thin film devices like FeCoB/MgO/FeCoB.[37,38] More importantly, such an FGT-based magnetic memory device is highly energy-efficient. For example, the well-known FeCoB/MgO/FeCoB based

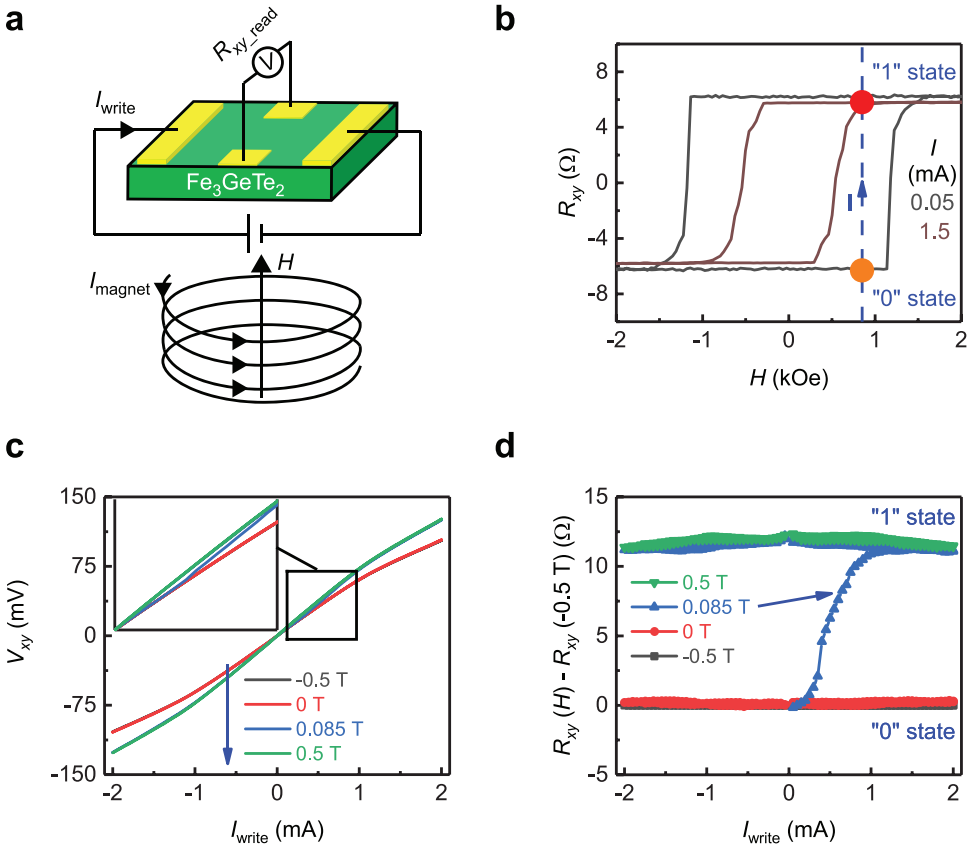

Figure 4. FGT-based magnetic memory. a) Schematic of the magnetic memory device. The magnetic information can be written by the current I_{write} and read by transverse Hall resistance R_{xy}. b) For sample S1, it illustrates the transition from "0" to "1" state under 0.085 T. The blue arrows indicate the writing path I of magnetic information. c) Measured Hall voltage (V_{xy}) as a function of I_{write} (0→ 2→ −2 → 2 mA) under various magnetic fields from −0.5 to 0.5 T (the blue arrow indicates the measurement sequence). The inset is a magnified view for the black box where the deviation under 0.085 T is clearer. d) $R_{xy}(H)$ − R_{xy}(−0.5 T) defined as ($V_{xy}(H)$ − V_{xy}(−0.5 T))/I_{write} as a function of I_{write} (0→ 2→ −2 → 2 mA) under various magnetic field from −0.5 T to 0.5 T. The blue arrow indicates the transition from "0" to "1" state while ramping I_{write} from 0 to 2 mA under 0.085 T.

© 2020 Wiley-VCH GmbH

SOT-MRAM[39] requires an extremely high current density of >400 mA μm^{-2} to switch the magnetization, which is about 80 times larger than that in our FGT device of ≈5 mA μm^{-2} (corresponds to ≈1 mA here).

In summary, we demonstrate the current control of the coercive field for nm-thin FGT, a 2D vdW topological ferromagnetic metal. We show that the observed current control is consistent with the unique properties of the SOT in FGT, and the gigantic SOT field is mainly due to the large Berry curvature of this topological material. We also successfully present a novel type of robust nonvolatile magnetic memory based on the giant SOT effect of FGT by using a tiny current. Our findings open up a fascinating avenue of electrical modulation and spintronic applications using 2D magnetic vdW materials.

Experimental Section

Sample Growth and Device Fabrication: FGT single crystals were grown by the chemical vapor transport method with iodine as the transport agent. High-purity elements (Fe, Ge, and Te) were stoichiometrically mixed and sealed in an evacuated quartz tube. The crystals were grown in a two-zone furnace with a temperature gradient of 750 °C (source) to 680 °C (sink) for 7 days.

To minimize the sample oxidation and degradation, all the FGT nanoflakes were exfoliated from the as-grown single crystals onto 285 nm SiO_2/Si substrates inside the glove box (O_2: <0.6 ppm; H_2O: <0.2 ppm) by a conventional mechanical exfoliation method with Scotch tape. Before taken out of the glove box, the samples were sealed in a vacuum plastic package to prevent degradation due to air. Before the standard electron-beam lithography (EBL), the spin-coated PMMA polymer on FGT was prebaked with a relatively moderate condition: 130 °C for 1.5 min. To reduce the sample oxidation and degradation of FGT nanoflake, 90/5 nm Au/Ti electrodes were deposited by the electron beam evaporation under a high vacuum (<10^{-5} Pa) immediately after EBL. During the whole process, including the transport measurements, the FGT samples were exposed to air for less than ≈25 min. Under this condition, the successfully measured FGT samples displayed typical and prominent R_{xy}–H hysteresis loops, without visible signs of considerable damage. In contrast, when the FGT sample was exposed to air for over 70 min in one of the control experiments, the sample was severely damaged. The measured R_{xx}–T curve shows a significantly insulating behavior, and the R_{xy}–H loop is too noisy to be a well-defined ferromagnetic hysteresis loop (Figure S9, Supporting Information).

Several FGT devices (samples S1, S2, S3, S4, S5, and S6 with a thickness of 21.3, 16.7, 6, 42, 17.5, and 15 nm, respectively) were fabricated. For the FGT/$NbSe_2$ heterostructure (sample S4), the $NbSe_2$ nanoflake was exfoliated onto a PDMS stamp and then dry transferred onto the SiO_2/Si substrate to form the FGT/$NbSe_2$ heterostructure.

Electrical Transport Measurements: Transport measurements with a Hall-bar geometry were made using a Quantum Design physical property measurement system with the highest magnetic field up to 9 T. Gold wires were used to make contacts between the chip carrier and the Au/Ti electrodes.

Theoretical Calculations: This section presents the calculated free energy barrier $M_sK_z^{\text{eff}}/2$ for the magnetization switching from $\mathbf{m}=-\hat{\mathbf{z}}$ to $\mathbf{m}=+\hat{\mathbf{z}}$. From the effective free energy density

$$f_{\text{eff}} = -\frac{M_s}{2}\left[K_z\cos^2\theta + \Gamma_0 J\sin^2\theta\cos\left(2\phi+\phi_J\right)\right] \quad (4)$$

it is evident that J does not affect f_{eff} for $\mathbf{m}=+\hat{\mathbf{z}}$ ($\theta = 0$) and $\mathbf{m}=-\hat{\mathbf{z}}$ ($\theta=\pi$). On the other hand, f_{eff} depends on φ for $\theta \neq 0, \pi$ (Figure 3b); f_{eff} as a function of φ is minimized for $\cos(2\phi+\phi_J)=\text{sgn}(\Gamma_0 J)$ and maximized for $\cos(2\phi+\phi_J)=-\text{sgn}(\Gamma_0 J)$. Thus for the unique value of φ that minimizes f_{eff}, f_{eff} becomes a function of θ only and is given by

$$f_{\text{eff}} = -\frac{M_s}{2}\left[K_z\cos^2\theta + |\Gamma_0 J|\sin^2\theta\right] = -\frac{M_s}{2}\left[\left(K_z - |\Gamma_0 J|\right)\cos^2\theta + |\Gamma_0 J|\right] \quad (5)$$

From this, one finds the free energy barrier of $M_sK_z^{\text{eff}}/2$ with the effective magnetic anisotropy K_z^{eff} given by

$$K_z^{\text{eff}} = K_z - |\Gamma_0 J| \quad (6)$$

During the preparation of the work, the reported modulation of coercivity in Fe_3GeTe_2/WTe_2 heterostructure in a very recent work was found.[40]

Supporting Information

Supporting Information is available from the Wiley Online Library or from the author.

Acknowledgements

The authors thank Kihoon Lee, Haleem Kim, and Nahyun Lee for their supports and helpful discussions. The authors also thank Dongjin Lee and Heedeuk Shin for their help with finite-element numerical calculations. IBS-CCES was supported by the Institute for Basic Science (IBS) in Korea (Grant No. IBS-R009-G1), and CQM was supported by the Leading Researcher Program of the National Research Foundation of Korea (Grant No. 2020R1A3B2079375). The theoretical works at the POSTECH were funded by Samsung Science and Technology Foundation (Grant No. BA-1501-07 & BA-1501-51). K.K. was supported by the National Research Foundation (NRF) Korea (Grant No. 2016R1D1A1B02008461), and internal R&D program at Korea Atomic Energy Research Institute (KAERI) (Grant No. 524210-20).

Conflict of Interest

The authors declare no conflict of interest.

Keywords

2D topological ferromagnetic metal Fe_3GeTe_2, current-tunable coercive field, magnetic van der Waals materials, spintronic and magnetic memory, unusually large spin–orbit torque

Received: June 16, 2020
Revised: September 25, 2020
Published online:

[1] J. G. Park, *J. Phys.: Condens. Matter* **2016**, *28*, 301001.
[2] C. T. Kuo, M. Neumann, K. Balamurugan, H. J. Park, S. Kang, H. W. Shiu, J. H. Kang, B. H. Hong, M. Han, T. W. Noh, J. G. Park, *Sci. Rep.* **2016**, *6*, 20904.
[3] J. U. Lee, S. Lee, J. H. Ryoo, S. Kang, T. Y. Kim, P. Kim, C. H. Park, J. G. Park, H. Cheong, *Nano Lett.* **2016**, *16*, 7433.
[4] B. Huang, G. Clark, E. Navarro-Moratalla, D. R. Klein, R. Cheng, K. L. Seyler, D. Zhong, E. Schmidgall, M. A. McGuire, D. H. Cobden, W. Yao, D. Xiao, P. Jarillo-Herrero, X. Xu, *Nature* **2017**, *546*, 270.
[5] C. Gong, L. Li, Z. Li, H. Ji, A. Stern, Y. Xia, T. Cao, W. Bao, C. Wang, Y. Wang, Z. Q. Qiu, R. J. Cava, S. G. Louie, J. Xia, X. Zhang, *Nature* **2017**, *546*, 265.

 © 2020 Wiley-VCH GmbH

[6] K. S. Burch, D. Mandrus, J. G. Park, *Nature* **2018**, *563*, 47.
[7] K. S. Novoselov, A. Mishchenko, A. Carvalho, A. H. Castro Neto, *Science* **2016**, *353*, aac9439.
[8] D. R. Klein, D. MacNeill, J. L. Lado, D. Soriano, E. Navarro-Moratalla, K. Watanabe, T. Taniguchi, S. Manni, P. Canfield, J. Fernandez-Rossier, P. Jarillo-Herrero, *Science* **2018**, *360*, 1218.
[9] T. Song, X. Cai, M. W. Tu, X. Zhang, B. Huang, N. P. Wilson, K. L. Seyler, L. Zhu, T. Taniguchi, K. Watanabe, M. A. McGuire, D. H. Cobden, D. Xiao, W. Yao, X. Xu, *Science* **2018**, *360*, 1214.
[10] S. Son, M. J. Coak, N. Lee, J. Kim, T. Y. Kim, H. Hamidov, H. Cho, C. Liu, D. M. Jarvis, P. A. C. Brown, J. H. Kim, C.-H. Park, D. I. Khomskii, S. S. Saxena, J.-G. Park, *Phys. Rev. B* **2019**, *99*, 041402.
[11] M. Gibertini, M. Koperski, A. F. Morpurgo, K. S. Novoselov, *Nat. Nanotechnol.* **2019**, *14*, 408.
[12] K. Kim, J. Seo, E. Lee, K. T. Ko, B. S. Kim, B. G. Jang, J. M. Ok, J. Lee, Y. J. Jo, W. Kang, J. H. Shim, C. Kim, H. W. Yeom, B. Il Min, B. J. Yang, J. S. Kim, *Nat. Mater.* **2018**, *17*, 794.
[13] C. Tan, J. Lee, S. G. Jung, T. Park, S. Albarakati, J. Partridge, M. R. Field, D. G. McCulloch, L. Wang, C. Lee, *Nat. Commun.* **2018**, *9*, 1554.
[14] Y. Deng, Y. Yu, Y. Song, J. Zhang, N. Z. Wang, Z. Sun, Y. Yi, Y. Z. Wu, S. Wu, J. Zhu, J. Wang, X. H. Chen, Y. Zhang, *Nature* **2018**, *563*, 94.
[15] S. Albarakati, C. Tan, Z. J. Chen, J. G. Partridge, G. Zheng, L. Farrar, E. L. H. Mayes, M. R. Field, C. Lee, Y. Wang, Y. Xiong, M. Tian, F. Xiang, A. R. Hamilton, O. A. Tretiakov, D. Culcer, Y. J. Zhao, L. Wang, *Sci. Adv.* **2019**, *5*, eaaw0409.
[16] M. Weisheit, S. Fahler, A. Marty, Y. Souche, C. Poinsignon, D. Givord, *Science* **2007**, *315*, 349.
[17] B. Huang, G. Clark, D. R. Klein, D. MacNeill, E. Navarro-Moratalla, K. L. Seyler, N. Wilson, M. A. McGuire, D. H. Cobden, D. Xiao, W. Yao, P. Jarillo-Herrero, X. Xu, *Nat. Nanotechnol.* **2018**, *13*, 544.
[18] S. Jiang, L. Li, Z. Wang, K. F. Mak, J. Shan, *Nat. Nanotechnol.* **2018**, *13*, 549.
[19] Z. Wang, T. Zhang, M. Ding, B. Dong, Y. Li, M. Chen, X. Li, J. Huang, H. Wang, X. Zhao, Y. Li, D. Li, C. Jia, L. Sun, H. Guo, Y. Ye, D. Sun, Y. Chen, T. Yang, J. Zhang, S. Ono, Z. Han, Z. Zhang, *Nat. Nanotechnol.* **2018**, *13*, 554.
[20] K. S. Burch, *Nat. Nanotechnol.* **2018**, *13*, 532.
[21] T. Maruyama, Y. Shiota, T. Nozaki, K. Ohta, N. Toda, M. Mizuguchi, A. A. Tulapurkar, T. Shinjo, M. Shiraishi, S. Mizukami, Y. Ando, Y. Suzuki, *Nat. Nanotechnol.* **2009**, *4*, 158.
[22] L. Liu, C. F. Pai, Y. Li, H. W. Tseng, D. C. Ralph, R. A. Buhrman, *Science* **2012**, *336*, 555.
[23] P. M. Haney, H.-W. Lee, K.-J. Lee, A. Manchon, M. D. Stiles, *Phys. Rev. B* **2013**, *87*, 174411.
[24] J. Yu, D. Bang, R. Mishra, R. Ramaswamy, J. H. Oh, H. J. Park, Y. Jeong, P. Van Thach, D. K. Lee, G. Go, S. W. Lee, Y. Wang, S. Shi, X. Qiu, H. Awano, K. J. Lee, H. Yang, *Nat. Mater.* **2019**, *18*, 29.
[25] X. Wang, J. Tang, X. Xia, C. He, J. Zhang, Y. Liu, C. Wan, C. Fang, C. Guo, W. Yang, Y. Guang, X. Zhang, H. Xu, J. Wei, M. Liao, X. Lu, J. Feng, X. Li, Y. Peng, H. Wei, R. Yang, D. Shi, X. Zhang, Z. Han, Z. Zhang, G. Zhang, G. Yu, X. Han, *Sci. Adv.* **2019**, *5*, eaaw8904.
[26] M. Alghamdi, M. Lohmann, J. Li, P. R. Jothi, Q. Shao, M. Aldosary, T. Su, B. Fokwa, J. Shi, *Nano Lett.* **2019**, *19*, 4400.
[27] Ø. Johansen, V. Risinggård, A. Sudbø, J. Linder, A. Brataas, *Phys. Rev. Lett.* **2019**, *122*, 217203.
[28] K. Garello, I. M. Miron, C. O. Avci, F. Freimuth, Y. Mokrousov, S. Blugel, S. Auffret, O. Boulle, G. Gaudin, P. Gambardella, *Nat. Nanotechnol.* **2013**, *8*, 587.
[29] S. Y. Park, D. S. Kim, Y. Liu, J. Hwang, Y. Kim, W. Kim, J. Y. Kim, C. Petrovic, C. Hwang, S. K. Mo, H. J. Kim, B. C. Min, H. C. Koo, J. Chang, C. Jang, J. W. Choi, H. Ryu, *Nano Lett.* **2020**, *20*, 95.
[30] G. Zheng, W.-Q. Xie, S. Albarakati, M. Algarni, C. Tan, Y. Wang, J. Peng, J. Partridge, L. Farrar, J. Yi, Y. Xiong, M. Tian, Y.-J. Zhao, L. Wang, *Phys. Rev. Lett.* **2020**, *125*, 047202.
[31] J. Kim, S. Son, M. J. Coak, I. Hwang, Y. Lee, K. Zhang, J.-G. Park, *J. Appl. Phys.* **2020**, *128*, 093901.
[32] Q. Li, M. Yang, C. Gong, R. V. Chopdekar, A. T. N'Diaye, J. Turner, G. Chen, A. Scholl, P. Shafer, E. Arenholz, A. K. Schmid, S. Wang, K. Liu, N. Gao, A. S. Admasu, S. W. Cheong, C. Hwang, J. Li, F. Wang, X. Zhang, Z. Qiu, *Nano Lett.* **2018**, *18*, 5974.
[33] D. Givord, Q. Lu, M. F. Rossignol, P. Tenaud, T. Viadieu, *J. Magn. Magn. Mater.* **1990**, *83*, 183.
[34] D. Givord, M. Rossignol, V. M. T. S. Barthem, *J. Magn. Magn. Mater.* **2003**, *258–259*, 1.
[35] N. H. D. Khang, Y. Ueda, P. N. Hai, *Nat. Mater.* **2018**, *17*, 808.
[36] D. Culcer, A. Cem Keser, Y. Li, G. Tkachov, *2D Mater.* **2020**, *7*, 022007.
[37] J. J. Bean, K. P. McKenna, *Phys. Rev. Mater.* **2018**, *2*, 125002.
[38] H. Bouchikhaoui, P. Stender, Z. Balogh, D. Baither, A. Hütten, K. Hono, G. Schmitz, *Acta Mater.* **2016**, *116*, 298.
[39] M. Cubukcu, O. Boulle, M. Drouard, K. Garello, C. O. Avci, I. M. Miron, J. Langer, B. Ocker, P. Gambardella, G. Gaudin, *Appl. Phys. Lett.* **2014**, *104*, 042406.
[40] Y. Shao, W. X. Lv, J. J. Guo, B. T. Qi, W. M. Lv, S. K. Li, G. H. Guo, Z. M. Zeng, *Appl. Phys. Lett.* **2020**, *116*, 092401.
[41] M. Dc, R. Grassi, J. Y. Chen, M. Jamali, D. Reifsnyder Hickey, D. Zhang, Z. Zhao, H. Li, P. Quarterman, Y. Lv, M. Li, A. Manchon, K. A. Mkhoyan, T. Low, J. P. Wang, *Nat. Mater.* **2018**, *17*, 800.

© 2020 Wiley-VCH GmbH